EFFECT OF IMPACT DAMAGE ON THE FATIGUE RESPONSE OF TiAl ALLOY – ABB-2

S. L. Draper, B. A. Lerch, J. M. Pereira, M V. Nathal
NASA – Glenn Research Center,Cleveland, OH 44135

M. Y. Nazmy, M. Staubli,
ALSTOM POWER, CH, Ltd., Borden CH5401 Switzerland

D. R. Clemens
Howmet Research Corp., Operhall Research Center, Whitehall, MI 49461

Abstract

The ability of γ - TiAl to withstand potential foreign or domestic object damage is a technical risk to the implementation of γ - TiAl in low pressure turbine (LPT) blade applications. In the present study, the impact resistance of TiAl alloy ABB-2 was determined and compared to the impact resistance of Ti-48Al-2Nb-2Cr [1]. Specimens were impacted with four different impact conditions with impact energies ranging from 0.22 to 6.09 J. After impacting, the impact damage was characterized by crack lengths on both the front and backside of the impact. Due to the flat nature of γ - TiAl's S-N (stress vs. cycles to failure) curve, step fatigue tests were used to determine the fatigue strength after impacting. Impact damage increased with increasing impact energy and led to a reduction in the fatigue strength of the alloy. For similar crack lengths, the fatigue strength of impacted ABB-2 was similar to the fatigue strength of impacted Ti-48Al-2Nb-2Cr [1], even though the tensile properties of the two alloys are significantly different. Similar to Ti-48Al-2Nb-2Cr, ABB-2 showed a classical mean stress dependence on fatigue strength. The fatigue strength of impacted ABB-2 could be accurately predicted using a threshold analysis.

Introduction

One of the technical risks of implementing γ - TiAl into service is its poor impact resistance in comparison to currently used nickel-based superalloys. The effect of ballistic impact damage on the fatigue strength of Ti-48Al-2Nb-2Cr (Ti-48-2-2) has been extensively studied [1]. The main conclusion of this report was that Ti-48Al-2Nb-2Cr 6th stage low pressure turbine (LPT) blades in a GE90 engine would survive an impact of normal service oriented conditions. It would take a large impact event, as might result from a catastrophic event, to cause impact damage large enough to fail a Ti-48Al-2Nb-2Cr LPT blade by service related fatigue. In this study, the effect of ballistic impact resistance on the fatigue strength of a different TiAl alloy, ABB-2, has been investigated and compared to the previous results on Ti-48Al-2Nb-2Cr. The TiAl alloy ABB-2 has a considerably different chemistry, microstructure, and mechanical properties compared to Ti-48Al-2Nb-2Cr. Of particular concern, ABB-2 has only half the ductility of Ti-48Al-2Nb-2Cr. Therefore, the ballistic impact resistance of ABB-2 was expected to be different from Ti-48Al-2Nb-2Cr.

Materials and Procedures

Impact specimens for both alloys were cast to size (Fig. 1) in a dog-bone configuration. Processing included hot isostatic pressing and heat treatment in a sequence typical for a LPT blade. Sample edges simulated the leading edges of actual LPT airfoils.

Static mechanical properties were measured using miniature tensile specimens machined by low stress grinding from the grip end of the impact specimens. The 51 mm long tensile samples had a 19 mm gage length and a 4 mm diameter and were tested in air at 23 and 650 °C using a constant strain rate of 1 x 10^{-4} s^{-1}.

The microstructure was studied using polarized light on an optical microscope. The Al content of the samples was determined by X-ray fluorescence (XRF) while the remaining elements were analyzed by inductively coupled plasma emission spectrometry (ICP) and gas analysis.

The ballistic impact rig consisted of a precision gun barrel mounted on a load frame with an attached furnace. The gun barrel was at a 90° angle to the width of the specimen and the end of the gun barrel was placed 4 mm away from the leading edge. The projectiles (BB's) were either 1.6 or 3.2 mm diameter steel ball bearings with a mass (m) of 0.0164 and 0.131 g, respectively. The kinetic impact energy was calculated based on $E=1/2mv^2$. The steel ball bearings were annealed for 1 h at 700 °C to reduce their hardness to ≤ 20 HRC, which is a hardness more representative of possible debris in an engine. The specimens were impacted at elevated temperature in air under a tensile stress of 70 MPa, simulating operating conditions for LPT blades. The specimens were impacted 3 times with one impact condition. Two impacts were placed on one edge of the sample separated by approximately 20 mm, and one additional impact was placed on the opposite edge, centered between the other two impacts (Fig. 1). The nominal distance from the leading edge to the impact center (denoted as X, Fig. 2) was 0.51 mm for the small projectile and 0.64 mm for the large projectile but specimen variability and an imprecise fit between the projectile and gun barrel resulted in some deviation in this distance. Six specimens were impacted at each of four impact conditions, Table I. The first three conditions in Table I were selected to duplicate conditions used for Ti-48Al-2Nb-2Cr [1] while the fourth condition was selected to simulate a higher temperature, higher energy impact event.

Table I. Impact and Fatigue Conditions

Impact Cond. #	Impact Temp. (°C)	BB Size (mm)	Velocity (m/s)	Energy (J)	Fatigue Temp. (°C)
1	260	1.6	162	0.22	650
2	260	1.6	301	0.75	650
3	260	3.2	152	1.53	650
4	730	3.2	300	6.09	730

Ballistic impact damage was characterized by measuring two surface crack lengths designated Hertzian (HZ) and backside straight (BS) crack length. These two crack lengths have been shown to be strongly correlated to remnant fatigue strength [1]. A HZ crack length was defined as the length of the longest crack on the impact side of the sample that was at an angle from the impact to the specimen edge, Fig. 2. BS crack length is the length from the specimen edge to the end of any cracking on the backside of the sample. As the distance from the center of the impact to the specimen edge (X) can affect the amount of impact damage and resulting fatigue strength, X was measured for every impact. Crack lengths for fatigue threshold analysis were measured on the fatigue fracture surfaces.

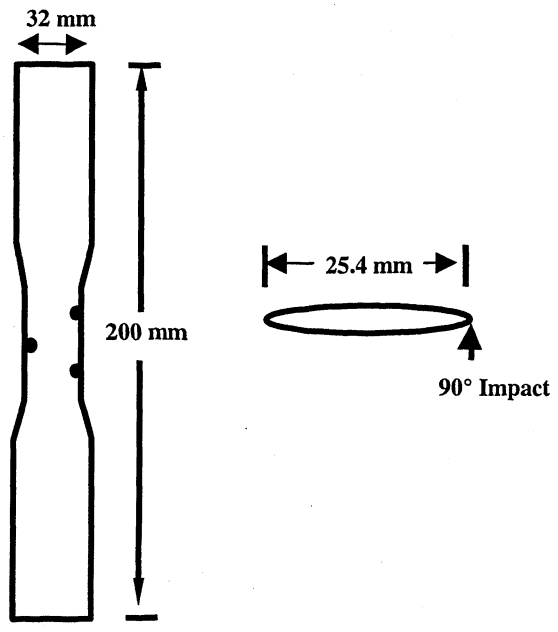

Figure 1. Cast-to-shape impact specimen design. Specimens impacted 90° to leading edge and at three locations, noted by dots.

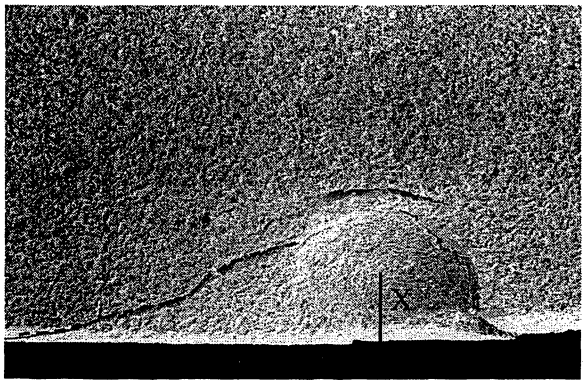

(a)

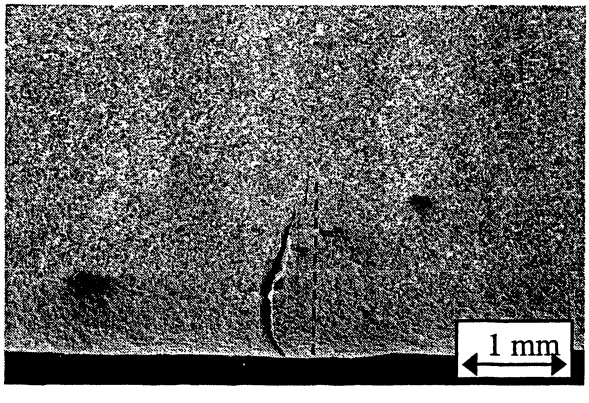

(b)

Figure 2. (a) Hertzian crack length (dashed line) measured on front (impact) side along with impact location distance, X, and (b) backside straight crack length on backside of sample.

High cycle fatigue tests of as-received and impacted samples were run at 650 or 730 °C with a frequency of 100 Hz. Fatigue crack growth rate is the highest at 650 °C for Ti-48Al-2Nb-2Cr [2] and therefore, this temperature was chosen for testing to simulate the worst-case scenario. The samples impacted with a high energy, 6.09 J, were fatigue tested at 730 °C in order to simulate a particular application. For each impact condition, three samples were fatigue tested with a load ratio, R, of 0.05 and the other three samples were tested at an R of 0.5. Due to the flat nature of γ - TiAl's S-N (stress vs. cycles to failure) curve, step fatigue tests were used to determine the maximum fatigue strength after impacting [3,4]. Based on the impact condition and previous experience, a starting stress level was chosen. If the sample survived either 10^6 or 10^7 cycles, the stress was increased by 7 to 14 MPa and run to failure or another 10^6 or 10^7 cycles. Fatigue strength was taken as the stress at the next to last step, i.e., the stress representing the fatigue threshold. The use of step fatigue testing avoided wasting a large number of samples due to run-outs as each sample was forced to fail.

Results and Discussion

Chemistry and Microstructure

The chemical compositions of ABB-2 and Ti-48-2-2 are given in Table II. The interstitial contents were within the specification range for both alloys. The microstructure of the ABB-2 samples tended to vary from the edge of the samples to the center. Near the edge, the microstructure was more lamellar with columnar grains (Fig. 3a) while in the center section, larger gamma grains were present surrounded by lamellar microstructure that had a more random orientation (Fig. 3b). The Ti-48Al-2Nb-2Cr had a typical duplex microstructure [1].

Table II. Alloy Chemistry

	Composition, at. %					
Alloy	Ti	Al	W	Si	Cr	Nb
ABB-2	50.6	46.5	2.28	0.48		
Ti-48-2-2	48.4	47.5			1.87	1.97

Tensile Properties

The tensile properties of specimens cut from the impact samples were typical for both alloys, Table III. The ABB-2 alloy has a considerably higher yield (σ_y) and ultimate tensile strength (σ_{UTS}) than Ti-48-2-2, but has only half the plastic elongation to failure (ε_p) at room temperature. At 650 °C, the ABB-2 alloy is still considerably stronger than Ti-48-2-2 but has less than half the ductility of Ti-48-2-2. The elastic moduli (E) are equivalent for both alloys at 23 and 650 °C.

Table III. Tensile Properties

Alloy	Temp. (°C)	σ_y (MPa)	σ_{UTS} (MPa)	ε_p (%)	E (GPa)
ABB-2	23	504	599	0.89	173
Ti-48-2-2	23	326	422	1.70	168
ABB-2	650	413	571	1.97	147
Ti-48-2-2	650	284	474	5.10	141

(a)

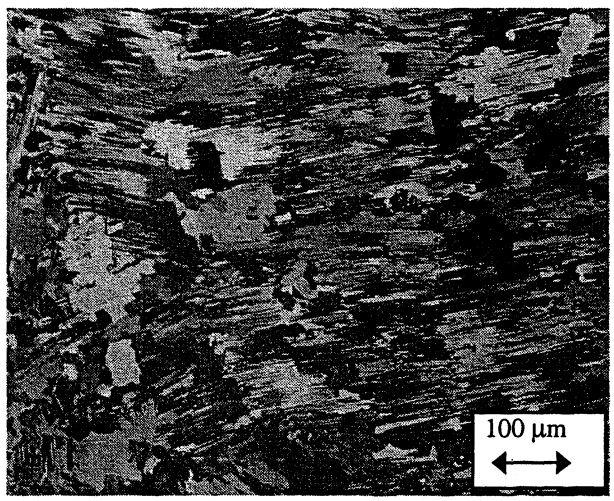

(b)

Figure 3. Microstructure of ABB-2 (a) near sample edge and (b) center of sample.

ABB-2 Crack Morphology

The type of impact damage produced depended on the energy level of the projectile. The low energy impacts, 0.22 J, resulted in shallow dents with very little cracking on the front side of the specimens. On the backside, the low energy impact resulted in an apparent crack for only half of the impacts. The backside cracks usually proceeded from the specimen edge to roughly the location opposite the impact crater. Backside cracks were semi-elliptical in shape and perpendicular to the loading axis of the fatigue specimen. Of the low energy impacts that did produce noticeable backside cracks, the cracks were narrow and less than 0.75 mm in length. At higher impact energies, front side circumferential cracks, also termed "Hertzian" cracks, initiated at the impact crater and grew towards the specimen edge, Fig. 2a. The HZ cracks extend into the thickness of the sample producing an expanding half-cone shape crack that resembles the Hertzian

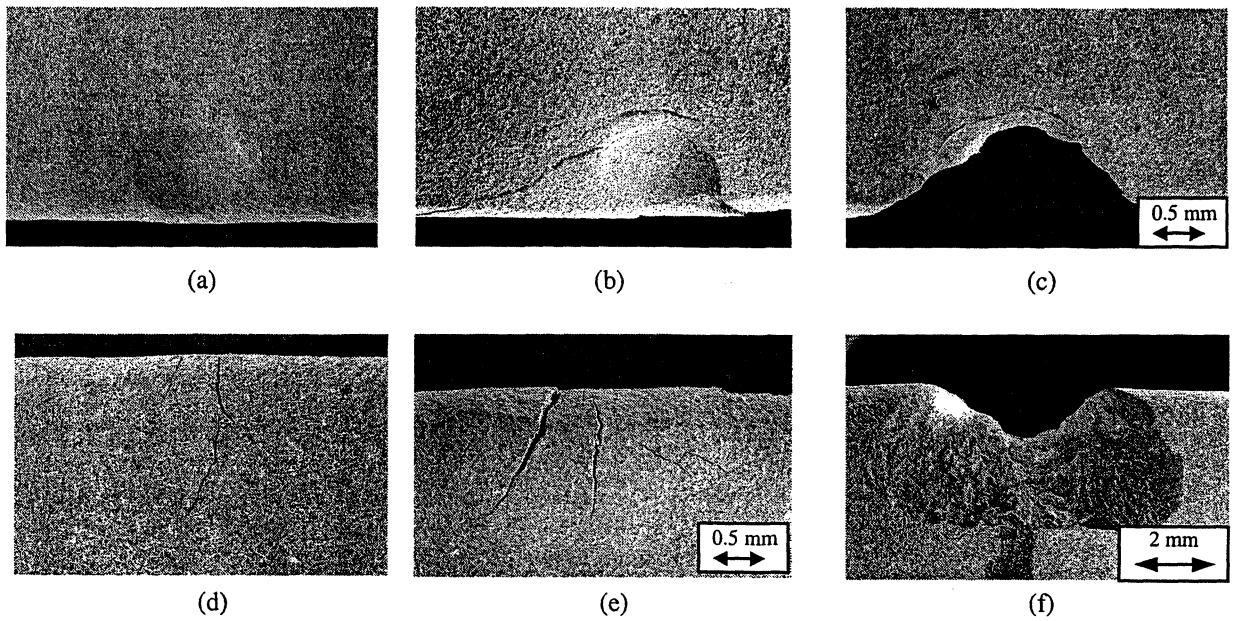

Figure 4. (a,b,c) Wide range of HZ crack lengths (0.48 to 3.1 mm) observed from impact condition #3 (Table I) for ABB-2 alloy. (d,e,f) Corresponding BS crack lengths were more consistent. (c, f) Front and backside of a "blow-out" illustrating half-cone shape of Hertzian crack.

cracks commonly observed in glass [5]. When HZ cracks propagate completely through the specimen a cone shaped chunk of material is completely removed and termed a "blow-out". An unusually wide range of front side impact damage occurred from the 1.5 J impacts with HZ crack lengths ranging from 0.48 to 4.2 mm, Fig. 4. Four of the twenty-four impacts were blown-out from the 1.5 J impacts. When the samples were not blown-out, the backside crack lengths were fairly consistent and ranged from 1.4 to 2.7 mm.

The Hertzian and backside straight crack lengths are plotted as a function of impact energy in Fig. 5 for both ABB-2 and Ti-48Al-2Nb-2Cr [1]. The level of impact damage was similar for ABB-2 and Ti-48-2-2 at similar impact energies. Both HZ and BS crack lengths increased with increasing impact energy up to 1.5 J. A significant increase in backside crack length occurs for blown-out samples due to the method of measurement. The BS crack lengths were measured from the leading edge to the end of the blowout on the backside, Fig. 4f, which is actually the backside of the HZ crack. The BS crack would have been smaller in length and contained in the blown-out portion. Impact condition #4 with a high impact temperature and a high impact energy of 6.09 J (Table I) resulted in all blow-outs. The HZ and BS cracks that resulted from the high temperature, high energy impacts were approximately the same length as the impacts from the 1.5 J energy impacts, Fig. 5, although the crack lengths had significantly less scatter. This is not unreasonable since once blow-outs start occurring higher energy levels will not create a larger blow-out. For larger blow-outs to occur, a larger value of X would be required. A small reduction in impact damage was observed in Ti-48-2-2 at elevated temperatures [1]; however, the extremely high impact energy of condition #4 overshadowed any benefit of the increased impact temperature.

The impact sites were polished from several angles to determine the effect of grain orientation on impact damage. Large lamellar grains were fairly common along the specimen surfaces, Fig. 3, but were not present for all of the samples. The large variability in HZ crack length may be attributed to the presence of these large grains at the specimen surface. The Hertzian cracks appeared to propagate readily when parallel to lamellae orientation as the crack path is straight and long in length, Fig. 6. Hertzian cracks that run perpendicular to lamellae have a more tortuous and shorter crack path. For the impact shown in Fig. 6, the longest HZ crack was on the right where the lamellae were oriented parallel to a typical crack path. On the left side of the impact, the lamellae were oriented at an angle to the typical crack path, and very little cracking occurred. BS crack length was not influenced by the grain size or orientation. For similar impact conditions, the BS crack length was very reproducible.

Impact crack morphology for ABB-2 was similar to the crack morphology of Ti-48Al-2Nb-2Cr at similar impact energies. As X, the distance from the leading edge to the center of the impact, can affect the crack lengths, only impacts in which X was within the range of 0.3 to 0.9 mm are shown in Figure 5. The crack length data for both alloys generally overlap. However, at the lowest impact energy, 0.22 J, half of the impacts on ABB-2 did not produce any apparent Hertzian or backside cracks whereas all of the 0.22 J impacts on Ti-48Al-2Nb-2Cr resulted in both front and backside cracks. Additionally, 26% of the 1.5 J impacts resulted in blow-outs for Ti-48Al-2Nb-2Cr compared to only 17% for ABB-2. This could be related to the higher strength of the ABB-2 alloy.

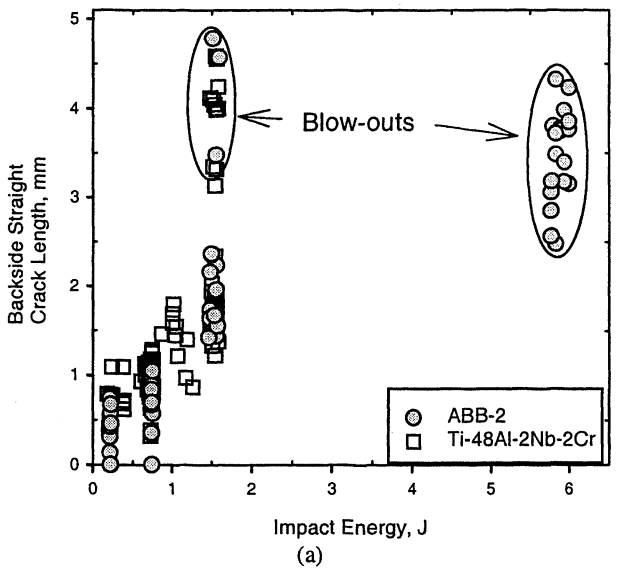

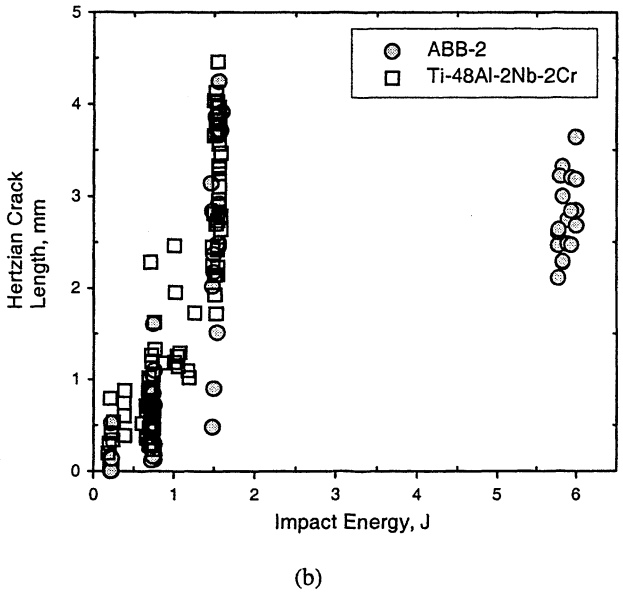

Figure 5. (a) Backside Straight and (b) Hertzian crack length as a function of impact energy.

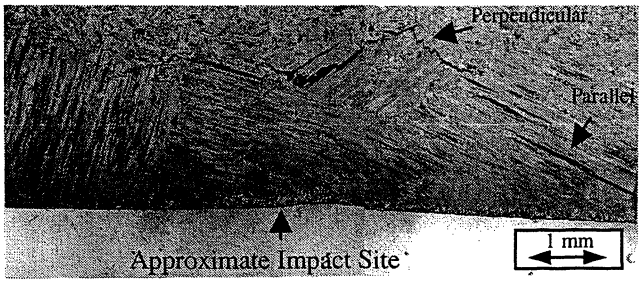

Figure 6. Hertzian cracks propagated easily parallel to lamellar grains but exhibited a more torturous crack path when perpendicular to lamellar grains.

The effect of impact parameters on HZ and BS crack lengths has been fitted for Ti-48Al-2Nb-2Cr using multiple regression techniques [1]. Three-dimensional representations of the equations are shown in Figure 7. These predictions are only valid for non-blown out impacts with impact energies from 0.22 to 2.0 J and X distances of up to 2.0 mm. For Ti-48Al-2Nb-2Cr, the X distance had a larger effect at high impact energy for both HZ and BS crack length. HZ crack length reached a maximum at an X distance of approximately 1.0 mm over the energy range tested. BS crack length also maximized at a X distance of 1.0 at low impact energies. However, at high impact energies, BS crack length continued to increase with increasing X. At a large enough X distance, the impacts should start to look like thick plate impacts which have a star shaped pattern on the backside instead of a backside crack coming into the width from the leading edge [6]. Insufficient data exists to formulate predictions for the ABB-2 alloy, however, the Ti-48Al-2Nb-2Cr equations were used to predict crack lengths for ABB-2 and the predicted crack lengths were compared to actual crack lengths. For HZ cracks, the large amount of scatter in actual crack lengths resulted in little correlation between predicted and actual crack lengths. However, a plot of measured BS versus predicted BS crack lengths resulted in a slope of 0.98 with a correlation coefficient of 81%. Therefore, the effect of impact energy, X distance, and presence of a blow-out on BS crack length for the ABB-2 alloy can be adequately predicted using the Ti-48Al-2Nb-2Cr model.

Effect of Impact Damage on Fatigue Strength

Specimens were impacted with energies as high as 6 J to determine the effect of impact energy on residual fatigue strength. In Fig. 8, the ordinate is the stress from the penultimate step and represents the fatigue threshold for a given level of impact damage. A stress at or below this level will not result in any crack growth out of the impact cracks and will lead to a run-out. Stresses above this level will result in crack growth and rapid failure of the sample. Since each of the three impacts on the sample have different crack lengths, only one of these cracks will exceed the threshold level first and propagate. The cracks from the other two impacts, as have been continuously observed, remain dormant during the fatigue test. Figure 8 shows that the fatigue strength of ABB-2 decreased with increasing impact energy (i.e., increasing crack size). While the data in Fig. 8 are for a load ratio of 0.05, the data for a load ratio of 0.5 show similar trends.

In general, specimens impacted at low energies failed at backside cracks, while at higher energies, the samples failed at HZ cracks. The transition in the failure initiation occurred at approximately 1 J. The fracture initiation sites were confirmed by observations of a bluish heat tint on the fracture surfaces of impacted samples after fatigue testing. The color change due to oxidation of impact-initiated cracks was clearly distinguishable from the yellowish color on the surface associated with fatigue crack propagation. The initiation site could also be distinguished by the shape of the fracture surfaces, Fig. 9. Backside cracks were elliptical in shape and flat fracture surfaces initiated from the backside of the impact, Fig. 9a. Hertzian cracks angled from the impact site to the backside of the sample, Fig. 9b. For samples in which fatigue failure initiated from the front side of the specimen, the fracture surface curved around the impact site, following the HZ crack [1].

At the center of the impact, the fatigue crack proceeded across the width of the specimen. Blowouts failed in a manner similar to the front-side initiated samples. Of the three indents per specimen, front- side-initiated failure generally occurred at the impact with the longest Hertzian crack. For backside initiated failure, the failure location was not consistently at the longest observed backside crack. This may be due to the surface roughness and difficulty observing the backside cracks. There were a number of samples that failed in a mixed mode, both backside and Hertzian cracks were visible on the fracture surface. For the mixed mode fractures, either the backside or Hertzian crack length was the longest of all three impacts. The cracks associated with the two impacts on each specimen that did not cause final fatigue failure were also inspected. There was no observable growth of these cracks during fatigue testing.

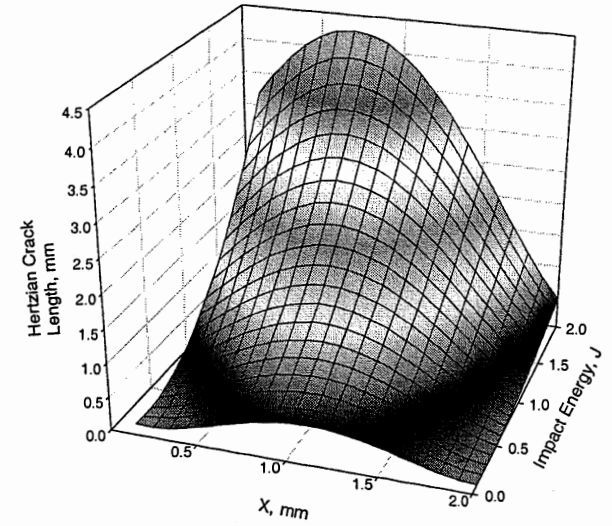

(a)

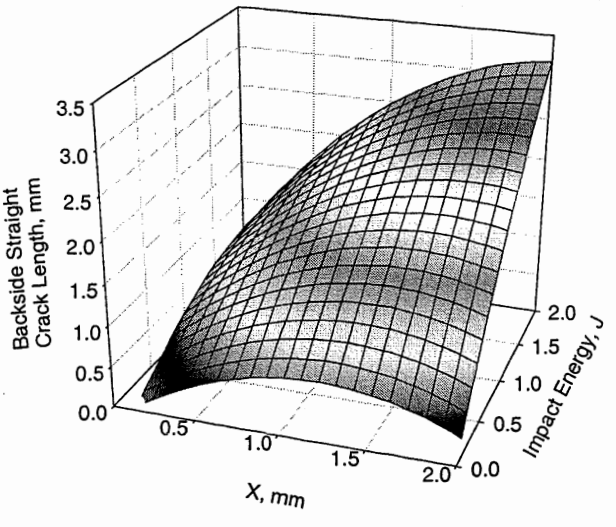

(b)

Figure 7 3-D plots depicting (a) Hertzian and (b) backside crack lengths for Ti-48Al-2Nb-2Cr over a large range of impact energy and X distance. Predictions are only valid for non-blown out samples.

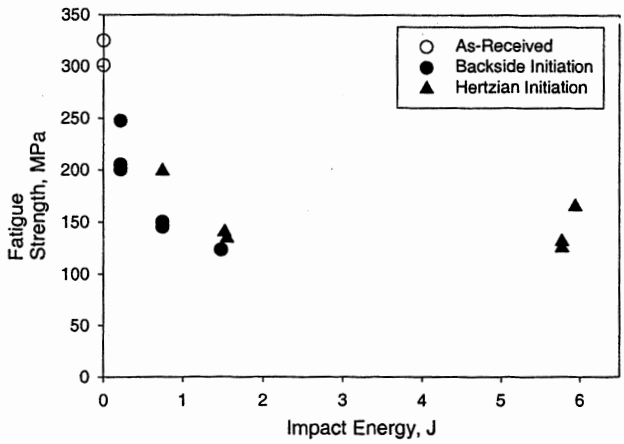

Figure 8 Effect of impact energy on fatigue strength. Fatigue initiation site changed from backside to Hertzian initiation with increasing impact energy. All data shown in this plot were generated at R = 0.05.

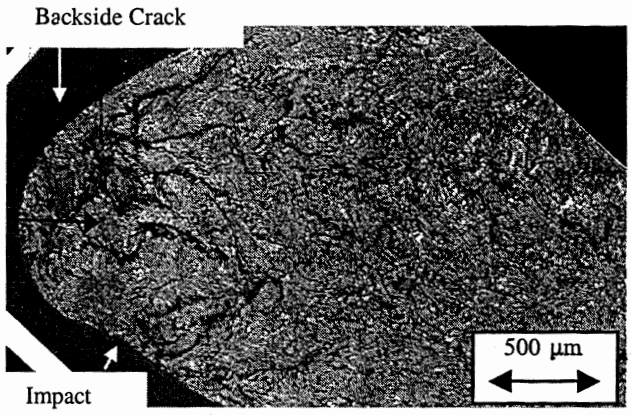

(a)

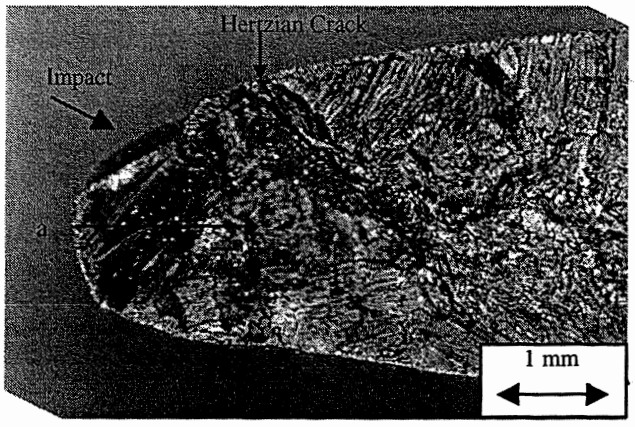

(b)

Figure 9. Fatigue fracture surfaces of (a) backside initiated, and (b) Hertzian initiated failure. Crack length, a, used for threshold analysis is shown for both backside and Hertzian initiated failures.

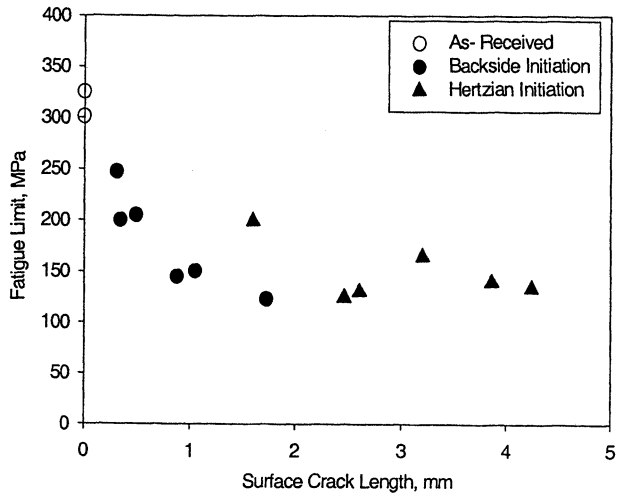

(a)

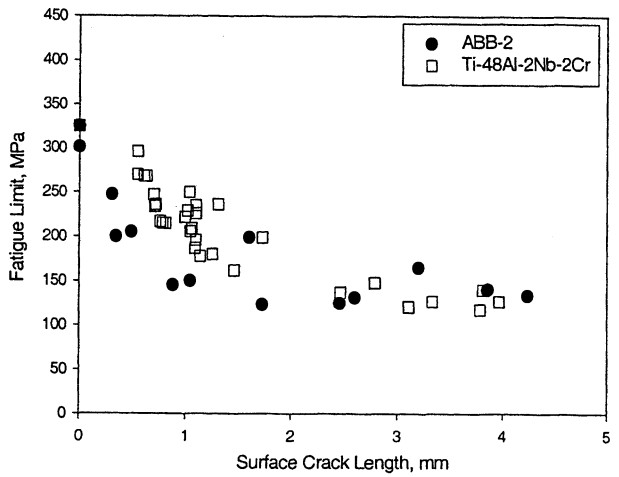

(b)

Figure 10. Fatigue limit decreased with increasing surface crack length for ABB-2 alloy (a). Fatigue limit of ABB-2 and Ti-48-2-2 [1] as a function of surface crack length (b).

The fatigue strengths for load ratios of 0.05 are plotted in Fig. 10 as a function of the surface-measured, crack length that initiated failure. As expected, the fatigue strength decreases with increasing crack length, and does so according to a $1/\sqrt{a}$ relationship as described by fracture mechanics.

The effect of surface crack length on fatigue strength for ABB-2 and Ti-48Al-2Nb-2Cr is compared in Fig. 10b. The 48-2-2 data show similar behavior to the ABB-2 material, particularly at larger initial crack lengths. However, the 48-2-2 has higher fatigue strength (approximately 50 MPa) at smaller crack lengths than the ABB-2 material

The effect of tensile mean stress on the fatigue strength of ABB-2 was evaluated. Three samples, impacted at the same temperature and impact energy, were tested at both load ratios (0.05, 0.5) for a total of 24 samples. The results show a classical mean stress dependence on the fatigue strength as shown using a Goodman Diagram, Figure 11. The data can be grouped according to their impact energy levels. At higher energy levels, the specimens can withstand less alternating stress per given mean stress and the curves shift downward. Also shown in this figure is a line representing fatigue data from smooth bar tests. This line lies significantly higher than the two virgin samples. The reason for this difference is currently unknown but may have to do with differences in the specimen geometry, the very large grains on the surface of the impact samples, and/or the surface roughness of the impact samples. The smooth bar data line extrapolates to a mean stress of 500 MPa, which is just slightly below the UTS of ABB-2. Curves for the impacted samples have been force fit through the 500 MPa point. Three different groups of energy levels were used for these fits: 0.2, 0.7 and a third group consisting of combined energies of 1.5 and 6 J. The large amount of scatter within any given energy level and the fact that only two load ratios were used made better fits impractical.

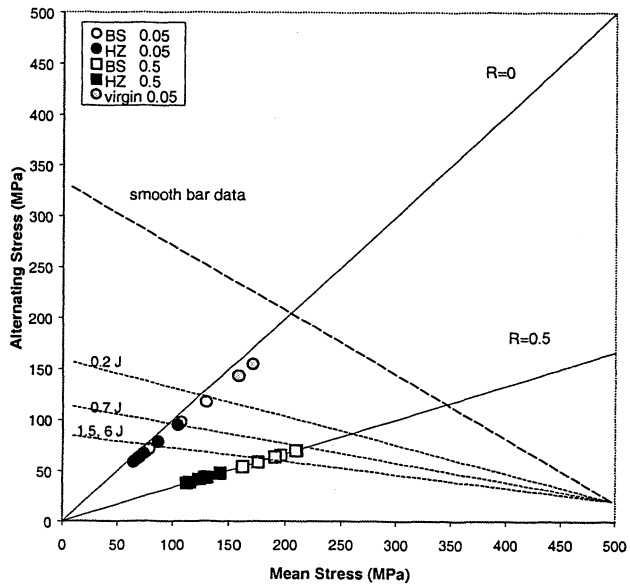

Figure 11 Goodman Diagram showing the effect of tensile mean stress on fatigue strength. Fatigue tests were run at 100 Hz and 650 or 730 °C. Curves for the impacted samples were force fit through the 500 MPa point.

A threshold analysis was performed on the ABB-2 data. Only the data for a load ratio of 0.05 were analyzed, although presumably the higher load ratio data can be analyzed by a similar method and corrected for the higher mean stress. Both the BS and HZ cracks were treated as Single Edge Notch (SEN) cracks. The stress intensity solution for the SEN was taken from [7]. The crack lengths used in the analysis for each type of cracks are shown in Fig. 9. While, geometrically, the BS cracks are not true through cracks, the SEN solution gave good results. It is believed that this solution "adjusts" for the elliptical-shaped leading edge that is not considered in the standard long-crack solutions, which assumes rectangular-shaped specimens.

The fatigue strength was predicted using the following equation:

$$\Delta\sigma_f = \frac{\Delta K_{th}}{f\sqrt{\pi a}}$$

where $\Delta\sigma_f$ is the fatigue strength (the maximum strength is used here since the minimum strength is nominally zero: R=0.05), a is the crack length as shown in Fig. 9, f is a geometric factor, and ΔK_{th} is the threshold stress intensity. For ABB-2 the threshold stress intensity factor was 9 $MPa\sqrt{m}$. The measured fatigue strength was compared to the predicted fatigue strengths in Fig 12. The SEN solution was shown to give good results for both the HZ and BS cracks. Data for both 650 and 730 C tests are combined in this figure, since the material has the same threshold stress intensity at these two temperatures.

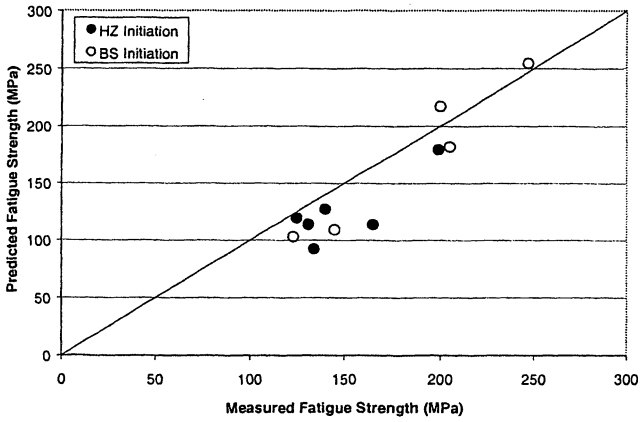

Figure 12. Predicted fatigue strength compared to measured fatigue strength for ABB-2. Specimens fatigue tested at 650 and 730 °C with a load ratio of 0.05. A threshold stress intensity factor of 9 $MPa\sqrt{m}$ was used to predict the fatigue strength.

Summary and Conclusions

Cast ABB-2 samples were impacted with four impact conditions and the level of impact damage increased with increasing impact energy. Considerable variation in front side or Hertzian crack length was observed and attributed to the large, lamellar grains that were present near the specimen surface in many samples. The extreme impact condition, 6.0 J of energy, resulted in all blow-outs but with crack lengths equal to the 1.5 J energy impacts. Similar ballistic impact conditions resulted in equivalent impact damage in ABB-2 and Ti-48Al-2Nb-2Cr alloys. The effect of impact conditions on the backside crack length of ABB-2 could be adequately predicted using crack length equations developed for Ti-48Al-2Nb-2Cr.

The fatigue strength of ABB-2 decreased with increasing impact energy. Generally, specimens impacted with low energies failed in fatigue from backside cracks whereas specimens impacted at high energies failed from the Hertzian cracks on the front side of the sample. The transition in fatigue initiation site occurred at approximately 1 J of impact energy. The fatigue strength decreased with increasing surface crack length according to the $1/\sqrt{a}$ relationship described by fracture mechanics. ABB-2 displayed a classical mean stress dependence on fatigue strength similar to Ti-48-2-2. A threshold analysis, using a stress intensity solution for single edge notch cracks, resulted in accurate predictions of fatigue strength. The fatigue strength of ABB-2 and Ti-48Al-2Nb-2Cr showed a similar dependence on external crack length, however, the 48-2-2 had a slightly higher fatigue strength at smaller crack lengths than the ABB-2 material The crack growth threshold primarily determines the fatigue life curve, therefore, to improve damage tolerance, an alloy with a higher crack growth threshold is required.

References

1. S. L. Draper, B. A. Lerch, J. M. Pereira, M.V. Nathal, C. M. Austin, and O. Erdman, "The Effect of Ballistic Impacts on the High Cycle Fatigue Properties of Ti-48Al-2Nb-2Cr (at. %), submitted to Metall. Trans. A.

2. J. M. Larsen, B. D. Worth, S. J. Balsone, and J. W. Jones, "An Overview of the Structural Capability of Available Gamma Titanium Aluminide Alloys", Gamma Titanium Aluminides, ed. Y. W. Kim, R. Wagner, and M. Yamaguchi (Warrendale, PA: The Minerals, Metals & Materials Society, 1995), 821-834.

3. J. A. Collins, Failure of Materials in Mechanical Design, (New York, NY: John Wiley and Sons, 1993).

4. J. Denk and S. Amhof, "Determination of the High Cycle Fatigue Strength with a Load-Increasing Single-Specimen Technique", Fatigue '96: Proc. Of 6th Int. Fatigue Cong., vol. III, ed. G. Lutjering and H. Nowack (Pergamon Press, 1996), 1967-1972.

5. H. Hertz, J. Reine Angew. Math., 92 (1881), pg. 156; translated and reprinted in English in "Hertz's Miscellaneous Papers," Macmillan, New York, 1996, Ch. 5.

6. P. S. Steif et al., "Surface Damage Due to Impact and Fatigue Strength Reduction in Gamma Titanium Aluminides," Structural Intermetallics, ed. M. V. Nathal, R. Darolia, C. T. Liu, P. L. Martin, D. B. Miracle, R. Wagner, and M. Yamaguchi (Warrendale, PA: The Minerals, Metals & Materials Society, 1997), 435-442.

7. H. Tada, P. C. Paris, G. R. Irwin, The Stress Analysis of Cracks Handbook, Second Edition, 1985, 2.10 – 2.11.